Journal of Sensor Science and Technology
Vol. 33, No. 5 (2024) pp. 326-337
http://dx.doi.org/10.46670/JSST.2024.33.5.326
pISSN 1225-5475/eISSN 2093-7563

MOS-based Gas Sensors for Early Alert of Thermal Runaway in Lithium-ion Batteries

Soo Min Lee[1,*], Seon Ju Park[1,*], and Ho Won Jang[1,2,+]

Abstract

The thermal runaway phenomenon in lithium-ion batteries hinders their large-scale application and leads to safety issues, including smoke, fire, and explosion. Therefore, early warning systems must be employed rapidly and reliably to ensure user safety, with methods for detecting gases such as hydrogen, carbon monoxide, and hydrocarbons—all indicators of the thermal runaway process—considered a promising approach. In particular, metal-oxide-semiconductor-based gas sensors can be used to monitor target gases owing to their high response, fast response, and facile integration. In this paper, we review various strategies for enhancing the performance of metal-oxide-semiconductor-based gas sensors, including nanostructure design, catalyst loading, and composite design. Future perspectives on employing metal-oxide-semiconductor-based gas sensors to monitor thermal runaway in lithium-ion batteries are also discussed.

Keywords: Gas sensors, Metal oxide semiconductors, Lithium-ion batteries, Thermal runaway, Hydrogen sensor, Carbon monoxide sensor, Hydrocarbon sensor

1. INTRODUCTION

Lithium-ion batteries (LIBs) have been extensively used as high-capacity rechargeable energy systems in electric vehicles and portable electronic devices owing to their high energy density, light weight, and long cycling life [1-3]. However, their high energy density and flammability pose safety concerns. In particular, under abusive conditions such as physical damage, overcharging, and extreme temperatures, they can undergo thermal runaway [4]. This process involves a rapid increase in temperature and gas venting, which can lead to fire or explosion. Considering preventing thermal runaway remains challenging, current strategies focus on delaying its onset and offering early alerts to allow users to respond. Thus, developing a promising system for early-stage monitoring of thermal runaway is essential to ensure user safety.

Indicators of thermal runaway include changes in temperature, voltage, pressure, and gas composition. As the temperature of the LIB increases, the materials within the cell begin to decompose, generating various gases (e.g., CO, H_2, CO, and C_xH_y) [5,6]. The accumulation of flammable gases in a cell, accompanied by increased temperature and pressure, can eventually result in an explosion or fire. Therefore, early detection of these gases is a promising pathway for providing warnings of thermal runaway. Moreover, providing a sensor platform with fast response speed and high reliability is crucial. Metal-oxide-semiconductor (MOS)-based gas sensors are promising platforms for gas detection owing to their high sensitivity, fast response/recovery speeds, small size, and cost-effectiveness [7-12]. These advantages render them suitable for detecting gases generated during the LIB thermal runaway process, thereby enabling early-stage alerts.

In this review, we present the factors that induce LIB thermal runaway and the gas generation process and demonstrate H_2, CO, and C_xH_y as thermal runaway indicators. We propose MOS-based gas sensors for the reliable detection of these gases owing to their inherent advantages. In addition, we discuss the operating mechanisms, current research trends, and development strategies of MOS-based sensors to provide early warnings of LIB thermal runaway.

2. THERMAL RUNAWAY IN LI-ION BATTERIES

2.1 Inducing factors of LIB thermal runaway

Thermal runaway is an uncontrollable positive feedback process, where increasing temperature accelerates further heat generation,

[1]Department of Materials Science and Engineering, Research Institute of Advanced Materials, Seoul National University
Seoul 08826, Republic of Korea
[2]Advanced Institute of Convergence Technology, Seoul National University
Suwon 16229, Republic of Korea
[+]Corresponding author: hwjang@snu.ac.kr
(Received: Aug. 12, 2024, Revised: Aug. 19, 2024, Accepted: Aug. 23, 2024)

potentially leading to fire or explosion. When the temperature rises beyond a certain point during the operation, the materials inside the LIB cell begin to decompose through exothermic reactions. As heat accumulates and its generation rate exceeds that of heat dissipation, the cell becomes increasingly unstable, ultimately causing an explosion. The thermal runaway of LIB can be triggered by three abusive conditions – mechanical, electrical, and thermal abuse [4,13,14]. These three abusing conditions are interrelated, which could ultimately develop to thermal abuse, consequently inducing the thermal runaway of betteries. Mechanical abuse by the external force causes the deformation or penetration of battery, triggering a short circuit which is a common feature of electrical abuse. In addition, overcharge/overdischarge, another feature of electrical abuse, can induce the formation of Li dendrite and separator damage, leading to a short circuit. The short circuit releases heat (e.g., Joule heat or chemical reaction heat), initiating thermal abuse. Thermal abuse may occur due to the local overheat caused by mechanical/electrical abuse or high ambient temperature. The thermal runaway proceeds in three steps; 1) the onset of overheating, 2) heat accumulation and gas release, and 3) combustion and explosion. During these steps, various signals, such as change in the electric signals, elevated temperature and generated gases, appear. Therefore, detecting the generated gases can be a promising way for monitoring of the early stage of thermal runaway.

2.2 Generation mechanism of gases during thermal runaway

LIBs undergo multiple reactions during the thermal runaway. When the temperature of a cell or a specific region inside the cell reaches a critical range, the components, including the solid electrolyte interface (SEI), separator, anode, cathode, and electrolyte, begin to decompose, resulting in exothermic breakdown. The rates of these reactions are precisely related to the exothermic self-heating rate, which increases exponentially with increasing temperature. The thermal runaway process in LIB generally involves six reaction steps: decomposition of the SEI, reactions between the anode and electrolyte, melting of the separator, decomposition of the cathode, decomposition of the electrolyte, and reactions between the binder and active materials in the cathode and anode (Fig. 1) [4,15].

Decomposition of SEI: At the initial stage of thermal runaway, the temperature of the LIB continued to increase. When the temperature reaches 70–90°C, the thin passivating SEI layer (e.g., ROCOOLi, Li_2CO_3, and ROLi) on the anode starts decomposing exothermically and releases a large amount of heat and gases (e.g., CO_2, O_2, and C_xH_y) [16,17]. The following equation takes ROCOOLi as an example:

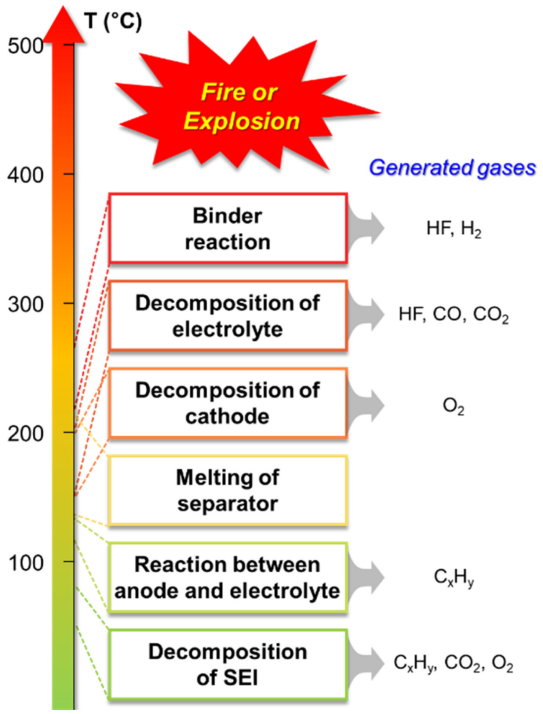

Fig. 1. Reaction process and release of gases during LIB thermal runaway.

$$(ROCOOLi)_2 \rightarrow Li_2CO_3 + C_2H_4\uparrow + CO_2\uparrow + \frac{1}{2}O_2\uparrow \quad (1)$$

Reaction between anode and electrolyte: When the temperature range reaches 120–140°C, the decomposition of the SEI layer is almost complete, leading to the direct exposure of the graphite anode to the electrolyte [18]. The heat generated from SEI decomposition causes a reaction between the intercalated Li ions in the anode and the organic solvents in the electrolyte, such as ethylene carbonate (EC), propylene carbonate (PC), and dimethyl carbonate (DMC), releasing flammable C_xH_y gases as follows [19-21]:

$$2Li + C_3H_4O_3(EC) \rightarrow Li_2CO_3 + C_2H_4\uparrow \quad (2)$$

$$2Li + C_4H_6O_3(PC) \rightarrow Li_2CO_3 + C_3H_6\uparrow \quad (3)$$

$$2Li + C_3H_6O_3(DMC) \rightarrow Li_2CO_3 + C_2H_6\uparrow \quad (4)$$

The intensity of the reactions in the process correlates with the extent of Li ion insertion into the anode, releasing more heat with

more pronounced reactions. Additionally, Li graphite reacts with the binder, resulting in heat generation.

Melting of separator: When the temperature reaches the melting point of the separator, the separator shrinks and melts, resulting in short circuits between electrodes. Commonly used separator materials include polyethylene (PE), polypropylene (PP), or ceramic-coated separators, which have melting points of ~135°C, 166°C, and 200°C, respectively [22]. This internal short circuit triggers the instantaneous release of a substantial amount of energy, exacerbating battery thermal runaway.

Decomposition of cathode: As the temperature increases and reaches a certain point during LIB thermal runaway, the active materials of the cathode become vulnerable to disproportionation, which causes their breakdown [23,24]. This process results in the release of significant amounts of reaction heat and oxygen, which induces the burning of the electrolyte and flammable gases inside the cell. Transition metal oxides such as $LiCoO_2$, $LiMn_2O_4$, $LiFePO_4$, and $LiNiO_2$ are commonly used as cathode materials. These decomposition reactions can be described using $LiCoO_2$ and $LiMn_2O_4$ as examples.

$$Li_xCoO_2 \rightarrow xLiCoO_2 + \left(\frac{1-x}{3}\right)Co_3O_4 + \left(\frac{1-x}{3}\right)O_2 \uparrow \quad (5)$$

$$LiMn_2O_4 \rightarrow LiMnO_2 + \frac{1}{3}Mn_3O_4 + \frac{1}{3}O_2 \uparrow \quad (6)$$

Decomposition of electrolyte: The decomposition of electrolyte salts (e.g., $LiPF_6$) accelerates when the temperature exceeds 150°C [25]. The generated PF_5 further accelerates the decomposition of the electrolyte and simultaneously reacts with H_2O, generating toxic HF. Using $LiPF_6$ as the electrolyte salt, the reaction is described as follows:

$$LiPF_6 \rightarrow LiF + PF_5 \quad (6)$$

$$PF_5 + H_2O \rightarrow POF_3 + 2HF \uparrow \quad (7)$$

Moreover, the electrolyte solvent (e.g., $C_6H_4O_3$) can react with the previously released oxygen at approximately 200°C, intensifying the thermal runaway by generating substantial heat and gases. During this process, considerable amounts of CO_2 and CO are released, as per the following equations:

$$\frac{5}{2}O_2 + C_6H_4O_3 \rightarrow 3CO_2 \uparrow + H_2O \quad (8)$$

(complete oxidation)

$$O_2 + C_6H_4O_3 \rightarrow 3CO \uparrow + 2H_2O \quad (9)$$

(incomplete oxidation)

As gas accumulates, the internal pressure of the battery cell increases rapidly, causing the battery to swell and eventually flushing the safety valve.

Binder reaction: When the temperature exceeds 260°C, binders can react with the anode or cathode, releasing a significant amount of H_2 and heat, as described in the following reactions (Eqs. 10–12) [26,27]. Commonly used binder materials include polyvinylidene fluoride (PVDF) and carboxymethyl cellulose (CMC), which stabilize the electrode structure.

$$-CH_2-CF_2 \rightarrow -CH=CF-HF \uparrow \quad (10)$$

$$-CH_2-CF_2 + Li \rightarrow LiF + -CH=CF- + 1/2H_2 \uparrow \quad (11)$$

$$CMC-OH + Li \rightarrow CMC-OH + 1/2H_2 \uparrow \quad (12)$$

These reactions are not completely independent and may occur spontaneously under certain conditions. Moreover, other reactions in LIB cells can cause thermal battery runaway. For instance, Galushkin et al. reported that the accumulation of H atoms in a graphite anode by repeated LIB cycles can cause complex exothermic reactions and generate massive amounts of H_2 and heat [28]. In addition, the combustion of graphite, the reaction between CO and H_2O, and the combustion of combustible gases can occur, releasing large amounts of CO_2, CO, or H_2.

2.3 Detectable gases during thermal runaway

Various gases, including O_2, CO_2, CO, C_xH_y, H_2, and HF, are generated during the LIB thermal runaway. Although a large amount of O_2 is released and can be easily detected by MOS-based sensors, detecting O_2 is not suitable for monitoring the early stages of LIB thermal runaway because of the fluctuation in the O_2 concentration owing to reactions with other released gases and the presence of external O_2 when the battery breaks. Additionally, detecting CO_2 via MOS-based sensors is challenging as it is a highly stable gas, thus making it difficult for it to react with the surface oxygen species of MOS. Furthermore, using HF as an indicator for early-stage thermal runways is impractical because the amount of released HF is too small, and its generation is limited to specific fluorine-containing batteries. Thus, O_2, CO_2, and HF were not considered as preferred indicators for the battery thermal runaway.

Recently, numerous attempts have been made to explore the types and amounts of gases produced during the thermal runaway of batteries. Koch et al. triggered thermal runaways in 51 different types of LIBs and analyzed the gases generated during this process [29]. They reported that the main released gases were CO_2 (36.56%), CO (28.38%), H_2 (22.27%), C_2H_4 (5.61%), CH_4 (5.26%), C_2H_6 (0.99%), C_3H_6 (0.52%), and other alkanes. Furthermore, Essl et al. conducted a self-made LIB thermal runaway reaction and analyzed the process using a gas-sensing platform [30]. The main detectable gases were CO_2, CO, H_2, and C_2H_4, along with small amounts of electrolyte vapor and water. Golubkov et al. demonstrated the thermal runaway characteristics of three types of commercial LIB and investigated the released gases using gas chromatography [6], with the results indicating that the commonly detected gas components were CO_2 (24.9–53%), H_2 (30.0–30.09%), CO (4.8–27.6%), CH_4 (4.1–8.6%), C_2H_4 (6.8–8.2%), and C_2H_6 (0.3–1.2%) with varying contents depending on the type of LIB. Given that H_2, CO, CH_4, and C_2H_4 are the most released gases during battery thermal runaway in detectable amounts, these gases can serve as indicators for early-stage battery thermal runaway.

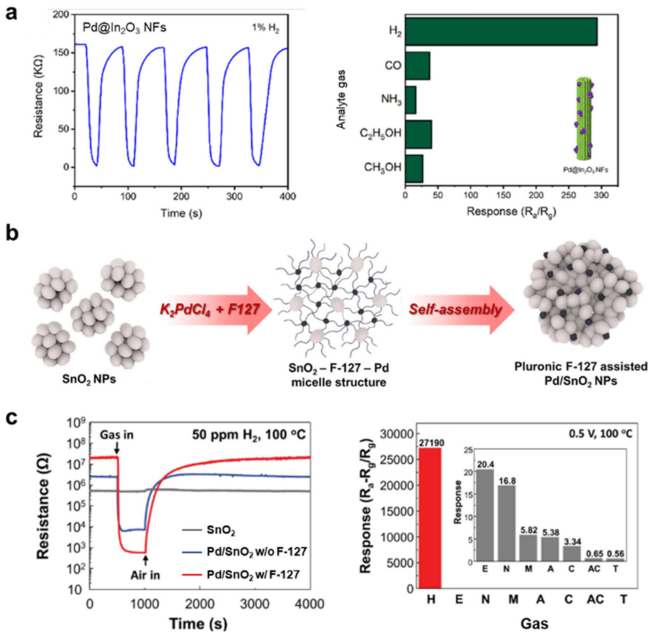

Fig. 2. (a) Gas response of Pd@In_2O_3 NFs sensor. Represented with permission from Ref. [43], Copyright (2022), American Chemical Society. (b) Synthesis process of F-127 assisted Pd/SnO_2 NPs, and (c) Gas response of F-127 assisted Pd/SnO_2 NPs (H: H_2, E: C_2H_5OH, N: NH_3, M: CH_3OH, C: CO, AC: CH_3COCH_3, T: C_7H_8). Represented with permission from Ref. [44], Copyright (2024), Elsevier.

3. METAL-OXIDE-SEMICONDUCTOR-BASED GAS SENSORS

Various gas-sensing techniques such as gas chromatography [31], fluorescent probes [32], photoacoustic spectroscopy [33], and non-dispersive infrared (NDIR) spectroscopy [34] have been investigated for detecting gases such as H_2, CO, and C_xH_y. Although these methods are highly accurate, they rely on complex, expensive, and bulky equipment, impeding the miniaturization and integration of sensors into portable applications. To overcome these challenges, MOS-based sensors have emerged owing to their distinct advantages, including easy integration, miniaturization, high sensitivity, fast response and recovery speeds, good reversibility, and cost effectiveness. In this section, we first discuss the gas-sensing mechanism of MOS-based sensors and introduce material design strategies for MOS-based sensors to detect thermal runaway indicator gases.

3.1. Gas-sensing mechanism of MOS-based gas sensors

MOS-based gas sensors gas sensors operate based on charge transfer during chemical reactions between surface oxygen species and analyte gases. MOSs are classified as n- and p-type semiconductors based on their major charge carriers (electrons for n-type semiconductors and holes for p-type semiconductors). At elevated temperatures (100–450°C), oxygen molecules are adsorbed on the MOS surface and form oxygen ion species (O_2^-, O^-, and O^{2-}) by taking electrons [35], resulting in the formation of electron depletion layers (EDLs) on the n-type MOS surface and hole accumulation layers (HALs) on the p-type MOS surface (Figs. 2 (a) and (b)). Upon exposure to reducing gases (e.g., CO, H_2, and CH_4), these gases are oxidized by ionized oxygen species, and electrons are injected into the EDL or HAL, allowing the resistance of the MOS to decrease (n-type) or increase (p-type) (Figs. 2 (c) and (d)). Therefore, the gas responses (S) are generally defined as R_a/R_g (n-type) or R_g/R_a (p-type), where R_a and R_g are the resistances of air and analyte gases, respectively. Other key evaluation parameters included selectivity, response/recovery times, and limit of detection (LOD). Selectivity, which refers to the ability of a sensor to accurately detect a target gas even in the presence of other interfering gases, is defined as the ratio of the target gas response to the interfering gas response ($S_{target}/S_{interferants}$). The response/recovery times are parameters used to evaluate the kinetics of the sensor upon exposure to the analyte gas. The

response time is the time required to reach 90% variation in resistance when the sensor is exposed to the analyte gas. Conversely, the recovery time is the time required for the sensor to return to 90% of its initial resistance in the absence of analyte gas. The LOD, i.e., the lowest measurable concentration of analyte gases required for reliable detection, is calculated from the correlation of gas concentration and response using criteria including $S > 1.2$ or a signal-to-noise ratio > 3 [36,37]. In the following section, we introduce various MOS-based gas sensors for monitoring LIB thermal runaway and discuss methodologies for enhancing sensor performance.

3.2. MOS-based gas sensors for thermal runaway monitoring

3.2.1. H_2 sensors

H_2 is a flammable and explosive gas with an explosion limit of 4% in air. H_2 is generated during LIB thermal runaway, mainly owing to the accumulation of H in the graphite anode and the reaction of Li with common electrode polymer binders (e.g., PVDF). Jin et al. overcharged a $LiFePO_4$-graphite battery pack and used sensors to detect the gas generated during the LIB thermal runaway [38]. The results indicated that H_2 could be detected 639 s and 769 s earlier than smoke and flame, respectively, demonstrating that H_2 detection is essential for ensuring safety. Therefore, employing H_2 sensors with high performance, such as high response, high selectivity, and fast response/recovery speed, is a viable strategy for monitoring the early stages of battery thermal runaway.

Various MOSs have been considered as H_2 sensing materials. For instance, Mineo et al. fabricated WO_3 nanorods (NRs) via hydrothermal methods to detect H_2 with fast response speed and high reliability at 350°C [39]. The WO_3 NRs sensor exhibited a rapid response time of 3 s and a linear response-concentration correlation at various concentrations (2000–50000 ppm). Liu et al. used a honeycombed SnO_2 as an ultrasensitive H_2 sensor [40]. The proposed sensor exhibited a high response of 8.4 with fast response and recovery times of 4 s and 10 s, respectively. Although MOS-based sensors exhibit a high response and rapid response/recovery kinetics, their lack of selectivity hinders their practical use, demonstrating that further improvements are necessary. Recently, incorporating noble metals has attracted significant attention for improving the H_2 sensing performances of MOS-based sensors. In particular, Pd catalysts have been used in numerous MOSs, such as In_2O_3, WO_3, and SnO_2, to achieve a high H_2 response and selectivity owing to their ability to dissociate H_2 into H atoms [41,42]. For instance, Chen et al. prepared Pd-loaded In_2O_3 nanofibers via electrospinning and wet impregnation to detect H_2 with ultrahigh response and selectivity at room temperature [43]. The proposed sensor exhibited ultrahigh H_2 selectivity ($S_{H2}/S_{others} > 7.4$) and a significantly high response (S_{H2} = 293.6) to 10,000 ppm of H_2 with short response and recovery times of 12 s and 23 s, respectively (Fig. 3 (a)). The intriguing H_2 sensing properties of Pd-In_2O_3 were driven by the catalytic effect of Pd on the dissociation of H_2 into H atoms and the expanded electron depletion layer due to the formation of a p-n heterojunction between p-type PdO and n-type In_2O_3. Moreover, our group reported Pd/SnO_2 nanoparticles (NPs) with maximized nanojunctions to achieve ultraselective and sensitive H_2 sensing properties [44]. The utilization of Pluronic F-127 in the synthesis of Pd/SnO_2 improved the dispersion and size control of the Pd nanoparticles, resulting in numerous heterojunctions between Pd and SnO_2 (Fig. 3 (b)). The as-synthesized Pd-SnO_2 with Pluoric F-127 exhibited ultrahigh selectivity ($S_{H2}/S_{others} > 1,332.8$) and significantly high response (S_{H2} = 27,190) to 50 ppm of H_2 at 100°C, even with a short response time of 3 s (Fig. 3 (c)). The significantly improved H_2 sensing performance was attributed to the increased catalytic activity of Pd due to size reduction, which showed an H_2 spillover effect, and the numerous nanojunctions between Pd and SnO_2.

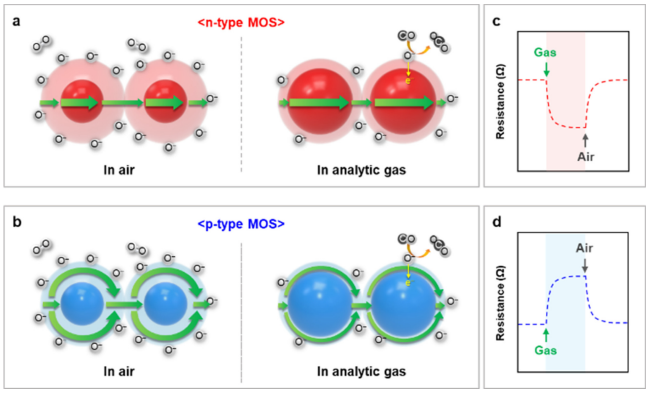

Fig. 3. Gas-sensing mechanism of MOS-based gas sensors

3.2.2. CO sensors

CO, one of the most common gases generated during battery thermal runaway, is released during the decomposition of the SEI and electrolyte solvent and the combustion of flammable gases. Therefore, accurate and rapid CO detection over a wide concentration range is crucial for monitoring the early stage of LIB thermal runaway.

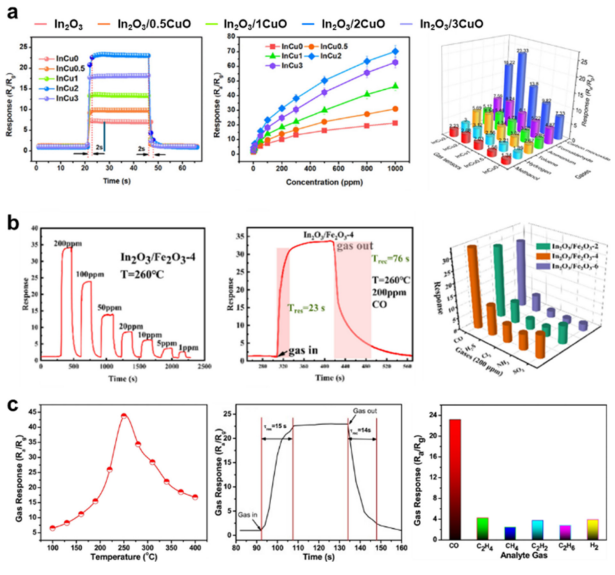

Fig. 4. (a) Gas response of In_2O_3/CuO based sensor. Represented with permission from Ref. [45], Copyright (2020), American Chemical Society. (b) Gas response of In_2O_3/Fe_2O_3 sensor. Represented with permission from Ref. [46], Copyright (2023), American Chemical Society. (c) Gas response of Pt/SnO_2 sensor. Represented with permission from Ref. [47], Copyright (2018), Elsevier.

Various MOS-based sensors such as SnO_2, In_2O_3, WO_3, and TiO_2 have garnered significant interest with regard to CO discrimination. However, owing to the small molecular weight of CO, its interaction with MOS-based sensors results in a low response because it reacts with a relatively low amount of surface oxygen species compared to other analyte gases (e.g., C_2H_5OH and C_xH_y). To overcome this limitation, MOSs have been functionalized with transition metal oxides and noble metal catalysts to facilitate their surface reaction with CO. Sun et al. fabricated an In_2O_3/CuO nanospheres via hydrothermal and calcination methods to detect CO with high sensitivity (Fig. 4 (a)) [45]. Compared to the pristine In_2O_3, the In_2O_3/CuO gas sensor exhibited a 3.3-fold higher response to CO (S_{CO} = 22.3 to 50 ppm CO) with a rapid response speed (response time = 2 s). The formation of p-n heterojunctions between p-type CuO and n-type In_2O_3 induces the expansion of the electron-depletion layer, resulting in a high CO response. Similarly, Zhao et al. incorporated Fe_2O_3 into In_2O_3 using a bimetallic-organic framework template to fabricate an effective CO sensor (Fig. 4 (b)) [46]. The In_2O_3/Fe_2O_3 core–shell nanotubes showed a response value of 33.7 to 200 ppm of CO with a response time of 26 s, demonstrating their practical use for real-time CO monitoring. They further assessed the CO selectivity over four interfering gases (Cl_2, H_2S, NH_3, and SO_2), and In_2O_3/Fe_2O_3 exhibited a high selectivity (S_{CO}/S_{others} > 2.9). The core–shell structure maximized the formation of an n-n heterojunction between In_2O_3 and Fe_2O_3, contributing to increased charge carrier density, thereby promoting the charge transfer between the analyte and sensing materials. Zhou et al. fabricated Pt NPs-decorated SnO_2 needles for CO gas sensors (Fig. 4 (c)) [47]. The Pt/SnO_2 sensor exhibited a high response to CO (S_{CO}= 23.18 to 100 ppm CO) with response and recovery times of 15 s and 14 s, respectively. The increased CO response is attributed to the chemical and electronic sensitizations of the Pt NPs. Zhang et al. prepared PtAg NPs-loaded WO_3 NRs for use as CO sensors [48]. The PtAg@WO_3 sensor demonstrated a high response to CO (S_{CO}= 2.79 to 100 ppm CO) with a fast response/recovery time of 75/24 s at 160°C. The enhanced CO sensing characteristics can be attributed to the chemical and electronic sensitization of PtAg. Noble metal catalysts increase the number of surface oxygen species through the O_2 spillover effect, thereby improving the CO response. Furthermore, the formation of PtO_x results in an increased electronic depletion layer, leading to a larger charge transfer variation. Although many attempts have been made to achieve highly sensitive CO detection with a rapid response speed, MOS-based sensors still encounter low selectivity problems, which require further improvement.

3.2.3. Hydrocarbon (C_xH_y) sensors

C_xH_y gases, such as CH_4 and C_2H_4, are produced during the decomposition of the SEI layer or formed during the reactions between the cathode and electrolyte. Thus, they can serve as indicators for the early-stage monitoring of LIB thermal runaway, although their proportions are not significantly higher than those of other gases (e.g., CO and H_2). Previous studies have reported developing various MOS-based sensors with a high response to C_xH_y by adding noble metal catalysts. These catalysts increase the number of surface oxygen species, thereby improving the oxidation of C_xH_y on the MOS surface. Yao et al. reported a Pd-SnO_2 nanoporous structure as a sensitive CH_4 sensor [49]. The sensor exhibited a high CH_4 response (S_{CH4} = 17.6 to 3000 ppm CH_4) with rapid kinetics (3 s and 5 s for response and recovery, respectively) at 340°C. Furthermore, Ivanov et al. prepared Pt-SnO_2 NPs for the sensitive detection of C_2H_4 [50]. The sensor showed a high response (S_{C2H4} = 9.8 to 100 ppm C_2H_4) at 450°C, while pristine SnO_2 exhibited a low response (S_{C2H4} = 1.42 to 100 ppm C_2H_4) to C_2H_4. However, for the practical use of sensors, a high selectivity for the target gas over other gases should be realized. Moon et al. reported a sensitive and selective C_2H_4 sensor with a Pd-V_2O_5-TiO_2/In_2O_3 bilayer structure (Fig. 5 (a))

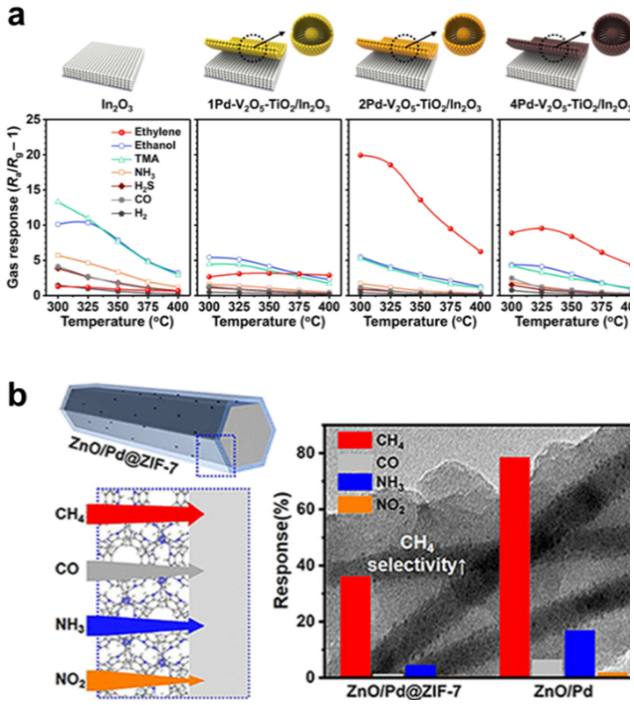

Fig. 5. (a) Gas response of Pd-V_2O_5-TiO_2/In_2O_3 sensor. Represented with permission from Ref. [51], Copyright (2023), The Royal Society of Chemistry. (b) Gas response of ZnO/Pd@ZIF-7 sensor. Represented with permission from Ref. [53], Copyright (2023), American Chemical Society.

[51]. The sensor exhibited a high C_2H_4 response (S_{C2H4} = 19.6 to 1 ppm C_2H_4) and selectivity (S_{C2H4}/S_{others}>4.5) at 325°C. The excellent sensing performance is attributed to the catalytic effect of the Pd-V_2O_5-TiO_2 overlayer, which facilitates the reforming of stable C_2H_4 into reactive CH_3CHO through a reaction known as heterogeneous Wacker oxidation. Similarly, Jeong et al. proposed a sensitive and selective C_2H_4 sensor using a Cr_2O_3/SnO_2 bilayer sensor [52]. Cr_2O_3/SnO_2 showed high response (S_{C2H4} = 16.8 to 2.5 ppm C_2H_4) and selectivity to C_2H_4 (S_{C2H4}/S_{others}>4.9) at 350°C. The catalytic Cr_2O_3 overlayer converted the less reactive C_2H_4 into more reactive species while oxidizing highly reactive interferents (e.g., C_2H_5OH, HCHO, and C_3H_9N), thereby improving the C_2H_4 sensing properties. These results indicated that controlling gas-reforming reactions using a catalytic overlayer is a promising method for achieving high sensitivity and selectivity for C_xH_y. Luo et al. proposed a ZnO/Pd@ZIF-7 core-shell structure as a selective CH_4 sensor (Fig. 5 (b)) [53]. This sensor achieved high selectivity of CH_4 over CO, NH_3, and NO_2 (S_{CH4}/S_{others}>8.0) and exhibited fast response/recovery kinetics (8.5/4.7 s) and good repeatability at 210°C. This high selectivity is explained by the adsorption of polar gases onto the ZIF-7 layers through which nonpolar CH_4 penetrates. Therefore, a molecular filtering layer can be adopted to achieve a high selectivity for C_xH_y.

4. FUTURE PERSPECTIVES

Nanostructure design, catalyst loading, and composite formation have significantly improved the performance of MOS-based gas sensors, including their response, selectivity, and response/recovery kinetics. Various MOS-based gas sensors for detecting LIB thermal runaway indicator gases are summarized in Table 1. Nonetheless, challenges remain for their use in actual applications, such as LIB thermal runaway monitoring. In particular, issues such as high power consumption, lack of reliability, and susceptibility to water poisoning should be addressed to improve the practicality of MOS-based sensors for the real-time monitoring of LIB thermal runaway.

MOS-based sensors often require an external heater because they are activated at high temperatures (> 150°C), leading to increased device sizes and high power consumption. To address this issue, microelectrochemical systems (MEMS) have been incorporated into MOS-based sensors [54,55]. The MEMS sensor platform comprises a microheater, a sensing material (MOS layer), and interdigitated electrodes with a 3-dimensional geometry. This platform enables mass production and realizes miniaturized and energy-saving sensing devices. For instance, Cho et al. adopted the MEMS platform on a SnO_2-ZnO-based H_2S sensor, which operates at 260°C, to decrease the power consumption to 6 mW (Fig. 6 (a)) [56]. Moreover, developing novel sensors operating under visible light is considered a promising approach to achieving energy savings [57-60]. For example, our group adopted blue micro-light-emitting diodes (μLEDs) onto a Pd-SnO_2 sensor to detect H_2 with an extremely low power consumption of 63.2 μW (Fig. 6 (b)) [61]. Although the H_2 response (S_{H2} = 0.5 to 50 ppm H_2) was not that high compared to other previously reported MOS-based sensors, this result still demonstrates the potential capability of using μLED platforms to establish advanced gas-sensing techniques.

To identify complex chemicals in the atmosphere, using multiple sensors with high selectivities toward different gases is essential. Pattern recognition technologies have enabled the precise discrimination of a mixture of gases in the atmosphere. Sung et al. fabricated 3×3 sensor arrays by loading different transition MOS (CuO, NiO, and Co_3O_4) and noble metal catalysts (Pt, Pd, and Au) onto SnO_2 NRs [62]. These nine sensors produced different eigengraphs for six gas species (CH_3COCH_3, C_7H_8, C_8H_{10}, C_2H_5OH, NH_3, and H_2S), which were analyzed using deep learning, achieving an accuracy of more than 99.5%.

Table 1. Summary of MOS-based gas sensors used for detecting LIB thermal runaway indicators

Gas	Material	Response (*S*) (Conc. [ppm])	Selectivity	Operating temp [°C]	LOD [ppm]	Response /recovery times [s]	Ref.
H_2	WO_3 NRs	1.5 (10,000)	> 1.3	350	1,076	5 / 71	[39]
	Honeycomb SnO_2	8.4 (1)	> 4.6	340	0.05	4 / 10	[40]
	Pd-In_2O_3 nanofibers	296.3 (10,000)	> 7.1	RT	–	12 / 23	[43]
	Pd/SnO_2 NPs	27,190 (50)	> 1332.8	100	4.5×10^{-5}	3 / –	[44]
CO	In_2O_3/CuO nanospheres	23.3 (100)	> 2.8	200	2.8	2 / 2	[45]
	In_2O_3/Fe_2O_3 core-shell nanotubes	33.7 (200)	> 2.9	260	1	26 / 76	[46]
	Pt-SnO_2 nanoneedles	23.2 (100)	> 5.5	250	–	15 / 14	[47]
	PtAg@WO_3 NRs	2.8 (100)	> 2.9	160	–	75 / 24	[48]
C_2H_4	Pt-SnO_2	9.8 (100)	–	450	–	–	[50]
	Pd-V_2O_5-TiO_2/In_2O_3 bilayer	19.6 (1)	> 4.5	325	7.3×10^{-3}	–	[51]
	Cr_2O_3/SnO_2 bilayer	16.8 (2.5)	> 4.9	350	2.4×10^{-2}	~ 60 / ~ 70	[52]
CH_4	ZnO/Pd@ZIF-7 core-shells	1.8 (500)	> 8.0	210	–	8.5 / 4.7	[53]
	Pd-SnO_2	17.6 (3000)	–	340	–	3 / 5	[49]

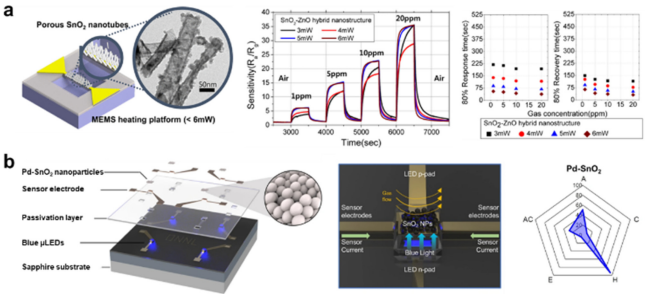

Fig. 6. (a) Schematic illustration of MEMS-based SnO_2-ZnO H_2S sensor, and its gas sensing properties. Represented with permission from Ref. [56], Copyright (2017), American Chemical Society. (b) Schematic illustration and OM image of Pd-SnO_2 sensor with μLEDs platforms, its gas sensing properties. Represented with permission from Ref. [61], Copyright (2024), Springer Nature.

Similarly, Moon et al. prepared a sensor array comprising nine sensors using three types of MOS (SnO_2, WO_3, and In_2O_3) with various nanostructures and catalyst loadings (Fig. 7 (a)) [63]. The responses of the sensors to eight different analytes (CH_3COCH_3, C_6H_6, CO, C_2H_5OH, H_2S, NH_3, and NO) were mapped onto a color scale and analyzed using principal component analysis (PCA). This sensor array can discriminate between the chemical vapors of H_2S, NH_3, and NO, even under humid conditions. These results highlight that using multiple sensors combined with pattern analysis is advantageous for precise discrimination of various gases.

Water is also generated during the LIB thermal owing to the decomposition of the electrolyte. Water poisoning degrades the performance of MOS-based chemoresistors, as they can be adsorbed onto the surface of sensing materials and form hydroxyls, hindering the generation of surface oxygen species. Thus, developing humidity-tolerant gas sensors is crucial for monitoring LIB thermal runaway. Various approaches have been explored to achieve this goal, including introducing water-resistant materials and additives that act as hydroxyl scavengers. For instance, Jeong et al. proposed a Tb_4O_7 overlaid In_2O_3 as a highly humidity-tolerant acetone sensor (Fig. 7 (b)) [64]. The inherent hydrophobic properties of Tb_4O_7 prevent water from approaching the In_2O_3 sensing layer. Similar effects have been

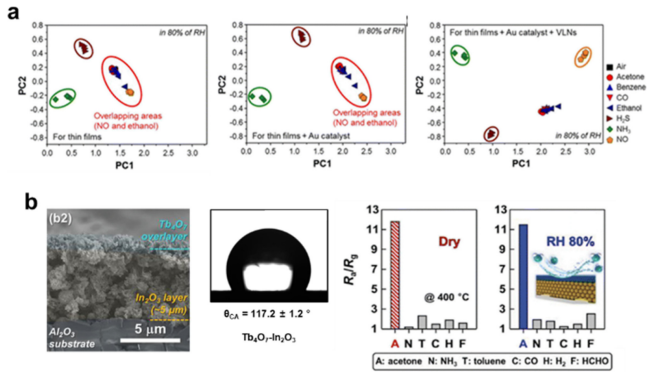

Fig. 7. (a) PCA plots of thin films, Au functionalized thin films, Au functionalized villi-like structure thin films with PC1 and PC2 using responses of 8 different analyte gases. Represented with permission from Ref. [63], Copyright (2016), American Chemical Society. (b) Material characterization of Tb_4O_7/In_2O_3 sensor and its gas sensing properties under dry and humid conditions. Represented with permission from Ref. [64], Copyright (2020), Wiley

observed with other hydrophobic materials such as ZIF-8 [65], FluoroPel [66], and PDMS [67]. Yoon et al. demonstrated that CeO_2 NPs can enhance the humidity resistance of In_2O_3 sensors [68]. The regenerative oxidation/reduction of Ce^{4+} and Ce^{3+} facilitates the hydroxyl radical scavenging reaction—a phenomenon also observed in multivalent metals and metal oxides, including Pr [69], NiO [70], and CuO [45]. Accordingly, incorporating appropriate materials into MOS-based sensors could be a viable solution for achieving humidity-tolerant sensors.

5. CONCLUSIONS

Considering the thermal runaway process in LIB must be identified at an early stage to ensure user safety, gas detection provides a reliable pathway for early-stage alerts for LIB thermal runaway. Detecting gases generated during LIB thermal runaway, such as H_2, CO, and C_xH_y, was achieved using the MOS. In this review, we described strategies for enhancing the performance of gas sensors (e.g., sensitivity, selectivity, and response/recovery kinetics). These methods include nanostructuring, catalyst decoration, and composite design. The potential and future perspectives of MOS-based sensors were also discussed. The development of MOS-based sensors will open a reliable pathway for early detection and prevention of thermal runaway, significantly enhancing the safety and reliability of LIB.

ACKNOWLEDGEMENT

S. M. Lee and S. J. Park contributed equally to this study. This work was financially supported in part by National R&D Program (RS-2024-00405016) through NRF (National Research Foundation of Korea), funded by the Ministry of Science and ICT, Republic of Korea. This work was also financially supported by "Cooperative Research Program for Agriculture Science and Technology Development (Project No. PJ01706703)"

REFERENCES

[1] J.-M. Tarascon and M. Armand, "Issues and challenges facing rechargeable lithium batteries", *Nature*, Vol. 414, No. 6861, pp. 359-367, 2001.

[2] A. Manthiram, "An outlook on lithium ion battery technology", *ACS Cent. Sci.*, Vol. 3, No. 10, pp. 1063-1069, 2017.

[3] G. Zubi, R. Dufo-López, M. Carvalho, and G. Pasaoglu, "The lithium-ion battery: State of the art and future perspectives", *Renew. Sustain. Energy Rev.*, Vol. 89, pp. 292-308, 2018.

[4] X. Feng, M. Ouyang, X. Liu, L. Lu, Y. Xia, and X. He, "Thermal runaway mechanism of lithium ion battery for electric vehicles: A review", *Energy Storage Mater.* Vol. 10, pp. 246-267, 2018.

[5] Z. Liao, J. Zhang, Z. Gan, Y. Wang, J. Zhao, T. Chen, and G. Zhang, "Thermal runaway warning of lithium-ion batteries based on photoacoustic spectroscopy gas sensing technology", *Int. J. Energy Res.*, Vol. 46, No. 15, pp. 21694-21702, 2022.

[6] A.W. Golubkov, D. Fuchs, J. Wagner, H. Wiltsche, C. Stangl, G. Fauler, G. Voitic, A. Thaler, and V. Hacker, "Thermal-runaway experiments on consumer Li-ion batteries with metal-oxide and olivin-type cathodes", *RSC Adv.* Vol. 4, No. 7, pp. 3633-3642, 2014.

[7] S. Y. Park, Y. Kim, T. Kim, T. H. Eom, S. Y. Kim, and H. W. Jang, "Chemoresistive materials for electronic nose: Progress, perspectives, and challenges", *InfoMat*, Vol. 1, No. 3, pp. 289-316, 2019.

[8] S.-Y. Jeong, "Recent advances and trends in filters for highly selective metal oxide gas sensors", *J. Sens. Sci. Technol.*, Vol. 33, No.1, pp. 48-55, 2024.

[9] S. M. Lee, Y. K. Moon, K. Lim, S.-W. Park, S. J. Park, T.-H. Kim, S. Y. Kim, J.-H. Lee, and Y.-M. Jo, "One-dimensional In_2O_3 nanofibers patterned onto functionalized catalytic electrodes: A novel approach for selective xylene detection", *Sens. Actuators B Chem.*, Vol. 382, p.133494, 2023.

[10] S. J. Park, Y. K. Moon, S.-W. Park, S. M. Lee, T.-H. Kim, S. Y. Kim, J.-H. Lee, and Y.-M. Jo, "Highly sensitive and selective real-time breath isoprene detection using the gas reforming reaction of MOF-derived nanoreactors", *ACS*

Appl. Mater. Interfaces, Vol. 15, No. 5, pp. 7102-7111, 2023.

[11] Y. Hu, W. Zheng, S. Fan, J. Zhang, and X. Liu, "Noble-transition-metal dichalcogenides-emerging two-dimensional materials for sensor applications", *Appl. Phys. Rev.*, Vol. 10, No. 3, 2023.

[12] J. P. Morán-Lázaro, M. Courel-Piedrahita, A. Guillén-Bonilla, F. López-Urías, H. Guillén-Bonilla, V. M. Soto-García, A. Palafox-Corona, and D. A. Hernández-Poot, "A novel sensor for the detection of n-butanol based on $CoMn_2O_4$ nanoparticles", *Electron. Mater. Lett.*, Vol.20, pp. 1-11, 2024.

[13] D. Ren, X. Feng, L. Liu, H. Hsu, L. Lu, L. Wang, X. He, and M. Ouyang, "Investigating the relationship between internal short circuit and thermal runaway of lithium-ion batteries under thermal abuse condition", *Energy Storage Mater.*, Vol. 34, pp. 563-573, 2021.

[14] Z. Wang, L. Zhu, J. Liu, J. Wang, and W. Yan, "Gas sensing technology for the detection and early warning of battery thermal runaway: a review", *Energy Fuels*, Vol. 36, No. 12, pp. 6038-6057, 2022.

[15] X. Feng, J. Sun, M. Ouyang, F. Wang, X. He, L. Lu, and H. Peng, "Characterization of penetration induced thermal runaway propagation process within a large format lithium ion battery module", *J. Power Sources*, Vol. 275, pp. 261-273, 2015.

[16] A. Kriston, I. Adanouj, V. Ruiz, and A. Pfrang, "Quantification and simulation of thermal decomposition reactions of Li-ion battery materials by simultaneous thermal analysis coupled with gas analysis", *J. Power Sources*, Vol. 435, p. 226774, 2019.

[17] R. Spotnitz and J. Franklin, "Abuse behavior of high-power, lithium-ion cells", *J. Power Sources*, Vol. 113, No.1, pp. 81-100, 2003.

[18] N. Tanaka and W. G. Bessler, "Numerical investigation of kinetic mechanism for runaway thermo-electrochemistry in lithium-ion cells", *Solid State Ion.*, Vol. 262, pp. 70-73, 2014.

[19] X. Tian, Y. Yi, B. Fang, P. Yang, T. Wang, P. Liu, L. Qu, M. Li, and S. Zhang, "Design strategies of safe electrolytes for preventing thermal runaway in lithium ion batteries", *Chem. Mater.*, Vol. 32, No. 23, pp. 9821-9848, 2020.

[20] H. Yang and X.-D. Shen, "Dynamic TGA–FTIR studies on the thermal stability of lithium/graphite with electrolyte in lithium-ion cell, *J. Power Sources*, Vol. 167, No. 2, pp. 515-519, 2007.

[21] M. Moshkovich, M. Cojocaru, H. Gottlieb, and D. Aurbach, "The study of the anodic stability of alkyl carbonate solutions by in situ FTIR spectroscopy, EQCM, NMR and MS", *J. Electroanal. Chem.*, Vol. 497, No. 1-2, pp. 84-96, 2001.

[22] C. J. Orendorff, "The role of separators in lithium-ion cell safety", *Electrochem. Soc. Interface*, Vol. 21, No. 2, pp. 61(1)-61(6), 2012.

[23] X. Zhu, Z. Wang, Y. Wang, H. Wang, C. Wang, L. Tong, and M. Yi, "Overcharge investigation of large format lithium-ion pouch cells with $Li(Ni_{0.6}Co_{0.2}Mn_{0.2})O_2$ cathode for electric vehicles: Thermal runaway features and safety management method", *Energy*, Vol. 169, pp. 868-880, 2019.

[24] Z. Wang, J. Yuan, X. Zhu, H. Wang, L. Huang, Y. Wang, and S. Xu, "Overcharge-to-thermal-runaway behavior and safety assessment of commercial lithium-ion cells with different cathode materials: A comparison study", *J. Energy Chem.*, Vol. 55, pp. 484-498, 2021.

[25] D. MacNeil and J. R. Dahn, "The reaction of charged cathodes with nonaqueous solvents and electrolytes: I. $Li_{0.5}CoO_2$", *J. Electrochem. Soc.*, Vol. 148, No. 11, p. A1205, 2001.

[26] P. Qin, Z. Jia, J. Wu, K. Jin, Q. Duan, L. Jiang, J. Sun, J. Ding, C. Shi, and Q. Wang, "The thermal runaway analysis on $LiFePO_4$ electrical energy storage packs with different venting areas and void volumes", *Appl. Energy*, Vol. 313, p. 118767, 2002.

[27] Z. Huang, C. Zhao, H. Li, W. Peng, Z. Zhang, and Q. Wang, "Experimental study on thermal runaway and its propagation in the large format lithium ion battery module with two electrical connection modes", *Energy*, Vol. 205, p. 117906, 2020.

[28] N. Galushkin, N. Yazvinskaya, and D. Galushkin, "Mechanism of thermal runaway in lithium-ion cells", *J. Electrochem. Soc.*, Vol. 165, No. 7, pp. A1303-A1308, 2018.

[29] S. Koch, A. Fill, and K.P. Birke, "Comprehensive gas analysis on large scale automotive lithium-ion cells in thermal runaway", *J. Power Sources*, Vol. 398, pp. 106-112, 2018.

[30] C. Essl, L. Seifert, M. Rabe, and A. Fuchs, "Early detection of failing automotive batteries using gas sensors", *Batteries*, Vol. 7, No. 2, pp. 25(1)-25(26), 2021.

[31] T. Ubuka, T. Abe, R. Kajikawa, and K. Morino, "Determination of hydrogen sulfide and acid-labile sulfur in animal tissues by gas chromatography and ion chromatography", *J. Chromatogr. B Biomed. Sci. Appl.*, Vol. 757, No. 1, pp. 31-37, 2001.

[32] N. Kumar, V. Bhalla, and M. Kumar, "Recent developments of fluorescent probes for the detection of gasotransmitters (NO, CO and H_2S)", *Coord. Chem. Rev.*, Vol. 257, No. 15-16, pp. 2335-2347, 2013.

[33] K. Chen, B. Zhang, S. Liu, and Q. Yu, "Parts-per-billion-level detection of hydrogen sulfide based on near-infrared all-optical photoacoustic spectroscopy", *Sens. Actuators B Chem.*, Vol. 283, pp. 1-5, 2019.

[34] T.-V. Dinh, I.-Y. Choi, Y.-S. Son, and J.-C. Kim, "A review on non-dispersive infrared gas sensors: Improvement of sensor detection limit and interference correction", *Sens. Actuators B Chem.*, Vol. 231, pp. 529-538, 2016.

[35] H.-J. Kim and J.-H. Lee, "Highly sensitive and selective gas sensors using p-type oxide semiconductors: Overview", *Sen. Actuators B Chem.*, Vol. 192, pp. 607-627, 2014.

[36] Y. G. Song, J. Y. Park, J. M. Suh, Y.-S. Shim, S. Y. Yi, H. W. Jang, S. Kim, J. M. Yuk, B.-K. Ju, and C.-Y. Kang, "Heterojunction based on Rh-decorated WO_3 nanorods for morphological change and gas sensor application using the transition effect", *Chem. Mater.*, Vol. 31, No. 1, pp. 207-215, 2018.

[37] S.-Y. Jeong, Y. K. Moon, J. Wang, and J.-H. Lee, "Exclusive detection of volatile aromatic hydrocarbons using bilayer oxide chemiresistors with catalytic overlayers", *Nat. Commun.*, Vol. 14, No. 1, pp. 233(1)-233(13), 2023.

[38] Y. Jin, Z. Zheng, D. Wei, X. Jiang, H. Lu, L. Sun, F. Tao, D. Guo, Y. Liu, and J. Gao, "Detection of micro-scale Li dendrite via H_2 gas capture for early safety warning", *Joule*, Vol. 4, No. 8, pp. 1714-1729, 2020.

[39] G. Mineo, K. Moulaee, G. Neri, S. Mirabella, and E. Bruno, "H_2 detection mechanism in chemoresistive sensor based on low-cost synthesized WO_3 nanorods", *Sens. Actuators B Chem.*, Vol. 348, p. 130704, 2021.

[40] L. Liu, C. Liu, S. Li, L. Wang, H. Shan, X. Zhang, H. Guan, and Z. Liu, "Honeycombed SnO_2 with ultra sensitive properties to H_2", *Sens. Actuators B Chem.*, Vol. 177, pp. 893-897, 2013.

[41] S. H. Cho, J. M. Suh, B. Jeong, T. H. Lee, K. S. Choi, T. H. Eom, T. Kim, and H. W. Jang, "Fast responding and highly reversible gasochromic H_2 sensor using Pd-decorated amorphous WO_3 thin films", *J. Chem. Eng.*, Vol. 446, p. 136862, 2022.

[42] P. Sermon and G. Bond, "Hydrogen spillover", *Catal. Rev.*, Vol. 8, No. 1, pp. 211-239, 1974.

[43] C. Chen, W. Chen, Q. Liu, Y. Liu, G. Xiao, C. Chen, F. Li, and J. Zhou, "Electrospinning of Pd–In_2O_3 nanofibers for high-performance room temperature hydrogen sensors", *ACS Appl. Nano Mater.*, Vol. 5, No. 9, pp. 12646-12655, 2022.

[44] G. B. Nam, T. H. Eom, S. H. Cho, Y. J. Kim, S. Choi, W. S. Cheon, S. J. Park, M. Shokouhimehr, J. M. Suh, J.-E. Ryu, S. Park, H. K. Park, H. J. Kim, S. J. Kim, S. M. Lee, S. H. Park, L. Shiming, M.-H. Oh, Y. S. Huh, and H. W. Jang, "Maximized nanojunctions in Pd/SnO_2 nanoparticles for ultrasensitive and rapid H_2 detection", *J. Chem. Eng.*, Vol. 494, p. 153116, 2024.

[45] Y. Sun, Z. Zhao, K. Suematsu, P. Li, Z. Yu, W. Zhang, J. Hu, and K. Shimanoe, "Rapid and stable detection of carbon monoxide in changing humidity atmospheres using clustered In_2O_3/CuO nanospheres", *ACS Sens*. Vol. 5, No. 4, pp. 1040-1049, 2020.

[46] F. Zhao, W. Cao, P.-H. Wang, J. Wang, L. Yu, Z. Qiao, and Z.-J. Ding, "Fast and Sensitive Detection of CO by Bi-MOF-Derived Porous In_2O_3/Fe_2O_3 Core–Shell Nanotubes", *ACS Sens.*, Vol. 8, No. 12, pp. 4577-4586, 2023.

[47] Q. Zhou, L. Xu, A. Umar, W. Chen, and R. Kumar, "Pt nanoparticles decorated SnO_2 nanoneedles for efficient CO gas sensing applications", *Sens. Actuators B Chem.*, Vol. 256, pp. 656-664, 2018.

[48] Y. Zhang, Y. Wang, L. Zhu, R. Zhang, and J. Cao, "Enhanced CO sensing performance of WO_3 nanorods with PtAg nanoparticles modification: A combined experimental and first-principle study", *Vacuum*, Vol. 193, p. 110526, 2021.

[49] L. Yao, Y. Li, Y. Ran, Y. Yang, R. Zhao, L. Su, Y. Kong, D. Ma, Y. Chen, and Y. Wang, "Construction of novel Pd–SnO_2 composite nanoporous structure as a high-response sensor for methane gas", *J. Alloys Compd.*, Vol. 826, p. 154063, 2020.

[50] P. Ivanov, E. Llobet, A. Vergara, M. Stankova, X. Vilanova, J. Hubalek, I. Gracia, C. Cané, and X. Correig, "Towards a micro-system for monitoring ethylene in warehouses, *Sens. Actuators B Chem.*, Vol. 111, pp. 63-70, 2005.

[51] Y. K. Moon, J. H. Kim, S.-Y. Jeong, S. M. Lee, S. J. Park, T. H. Kim, J.-H. Lee, Y. C. Kang, "Exclusive detection of ethylene using metal oxide chemiresistors with a Pd–V_2O_5–TiO_2 yolk–shell catalytic overlayer via heterogeneous Wacker oxidation", *J. Mater. Chem. A*, Vol. 11, No. 2, pp. 666-675, 2023.

[52] S.-Y. Jeong, Y. K. Moon, T.-H. Kim, S.-W. Park, K. B. Kim, Y. C. Kang, and J.-H. Lee, "A new strategy for detecting plant hormone ethylene using oxide semiconductor chemiresistors: exceptional gas selectivity and response tailored by nanoscale Cr_2O_3 catalytic overlayer", *Adv. Sci.*, Vol. 7, No. 7, p. 1903093, 2020.

[53] S. Luo, R. Chen, J. Wang, and L. Xiang, "ZnO/Pd@ ZIF-7-based gas sensors for selective methane sensing, *ACS Appl. Nano Mater.*, Vol. 6, No. 7, pp. 5808-5816, 2023.

[54] W. Yan, H. Xu, M. Ling, S. Zhou, T. Qiu, Y. Deng, Z. Zhao, and E. Zhang, "MOF-derived porous hollow Co_3O_4@ZnO cages for high-performance MEMS trimethylamine sensors", *ACS Sens.*, Vol. 6, No. 7, pp. 2613-2621, 2021.

[55] N. Luo, C. Wang, D. Zhang, M. Guo, X. Wang, Z. Cheng, and J. Xu, "Ultralow detection limit MEMS hydrogen sensor based on SnO_2 with oxygen vacancies", *Sens. Actuators B Chem.*, Vol. 354, p. 130982, 2022.

[56] I. Cho, K. Kang, D. Yang, J. Yun, and I. Park, "Localized liquid-phase synthesis of porous SnO_2 nanotubes on MEMS platform for low-power, high performance gas sensors", *ACS Appl. Mater. Interfaces*, Vol. 9, No. 32, pp. 27111-27119, 2017.

[57] J. M. Suh, T. H. Eom, S. H. Cho, T. Kim, and H. W. Jang, "Light-activated gas sensing: A perspective of integration with micro-LEDs and plasmonic nanoparticles", *Mater. Adv.*, Vol. 2, No. 3, pp. 827-844, 2021.

[58] K. Lim, Y. M. Jo, J. W. Yoon, J. S. Kim, D. J. Lee, Y. K. Moon, J. W. Yoon, J. H. Kim, H. J. Choi, and J. H. Lee, "A transparent nanopatterned chemiresistor: visible-light plasmonic sensor for trace-level NO_2 detection at room temperature", *Small*, Vol. 17, No. 20, p. 2100438, 2021.

[59] T. H. Eom, S. H. Cho, J. M. Suh, T. Kim, J. W. Yang, T. H. Lee, S. E. Jun, S. J. Kim, J. Lee, S.-H. Hong, and H. W. Jang, "visible light driven ultrasensitive and selective NO_2 detection in tin oxide nanoparticles with sulfur doping assisted by L-Cysteine", *Small*, Vol. 18, No. 12, p. 2106613, 2022.

[60] S. M. Majhi, A. Mirzaei, H. W. Kim, S. S. Kim, and T. W. Kim, "Recent advances in energy-saving chemiresistive gas sensors: A review", *Nano Energy*, Vol. 79, p. 105369, 2021.

[61] G.B. Nam, J.-E. Ryu, T.H. Eom, S.J. Kim, J.M. Suh, S. Lee, S. Choi, C.W. Moon, S.J. Park, S.M. Lee, B. Kim, S. H. Park, J. W. Yang, S. Min, S. Park, H. J. Kim, S. E. Jun, T. H. Lee, Y. J. Kim, J. Y. Kim, Y. J. Hong, J.-I. Shim, H.-G. Byun, Y. Park, I. Park, S.-W. Ryu, and H. W. Jang, "Real-time tunable gas sensing platform based on SnO_2 nanoparticles activated by blue micro-light-emitting diodes", *Nano Micro Lett.*, Vol. 16, No. 1, pp. 1-17, 2024.

[62] S.-H. Sung, J. M. Suh, Y. J. Hwang, H. W. Jang, J. G. Park, and S. C. Jun, "Data-centric artificial olfactory system based on the eigengraph", *Nat. Commun.*, Vol. 15, No. 1, p. 1211, 2024.

[63] H. G. Moon, Y. Jung, S. D. Han, Y.-S. Shim, B. Shin, T. Lee, J.-S. Kim, S. Lee, S. C. Jun, and H.-H. Park, "Chemiresistive electronic nose toward detection of biomarkers in exhaled breath", *ACS Appl. Mater. Interfaces*, Vol. 8, No. 32, pp. 20969-20976, 2016.

[64] S.-Y. Jeong, Y. K. Moon, J. K. Kim, S.-W. Park, Y. K. Jo, Y. C. Kang, and J.-H. Lee, "A general solution to mitigate water poisoning of oxide chemiresistors: bilayer sensors with Tb_4O_7 overlayer", *Adv. Funct. Mater.*, Vol. 31, No. 6, p. 2007895, 2021.

[65] G. S. Kim, Y. Lim, J. Shin, J. Yim, S. Hur, H. C. Song, S. H. Baek, S. K. Kim, J. Kim, and C. Y. Kang, "Breathable MOFs Layer on Atomically Grown 2D SnS_2 for Stable and Selective Surface Activation", *Adv. Sci.*, Vol. 10, No. 17, p.2301002, 2003.

[66] A. Kumar, P. Zhang, A. Vincent, R. McCormack, R. Kalyanaraman, H. J. Cho, and S. Seal, "Hydrogen selective gas sensor in humid environment based on polymer coated nanostructured-doped tin oxide", *Sens. Actuators B Chem.*, Vol. 155, No. 2, pp. 884-892, 2011.

[67] F. Qu, S. Zhang, C. Huang, X. Guo, Y. Zhu, T. Thomas, H. Guo, J. P. Attfield, and M. Yang, "Surface functionalized sensors for humidity-independent gas detection", *Angew. Chem.*, Vol. 60, No. 12, pp. 6561-6566, 2021.

[68] J.-W. Yoon, J.-S. Kim, T.-H. Kim, Y. J. Hong, Y. C. Kang, and J.-H. Lee, "A new strategy for humidity independent oxide chemiresistors: dynamic self-refreshing of In_2O_3 sensing surface assisted by layer-by-layer coated CeO_2 nanoclusters", *Small*, Vo. 11, No. 28, pp. 4229-4240, 2016.

[69] J.-S. Kim, C.W. Na, C.-H. Kwak, H.-Y. Li, J.W. Yoon, J.-H. Kim, S.-Y. Jeong, and J.-H. Lee, "Humidity-independent gas sensors using Pr-doped In_2O_3 macroporous spheres: role of cyclic Pr^{3+}/Pr^{4+} redox reactions in suppression of water-poisoning effect", *ACS Appl. Mater. Interfaces*, Vol. 11, No. 28, pp. 25322-25329, 2019.

[70] H.-R. Kim, A. Haensch, I.-D. Kim, N. Barsan, U. Weimar, and J.-H. Lee, "The role of NiO doping in reducing the impact of humidity on the performance of SnO_2-based gas sensors: synthesis strategies, and phenomenological and spectroscopic studies", *Adv. Funct. Mater.*, Vol. 21, No. 23 pp. 4456-4463, 2011.